1592
214
10-30-79

DR. 204 OCTOBER 1979

PPPL-1592
UC-20d,f

TECHNIQUES FOR MEASURING THE ALPHA-PARTICLE DISTRIBUTION IN MAGNETICALLY CONFINED PLASMAS

BY

D. E. POST, D. R. MIKKELSEN,
R. A. HULSE, L. D. STEWART,
AND J. C. WEISHEIT

PLASMA PHYSICS LABORATORY

MASTER

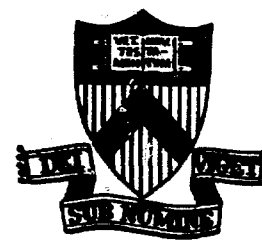

DISTRIBUTION OF THIS DOCUMENT IS UNLIMITED

PRINCETON UNIVERSITY
PRINCETON, NEW JERSEY

This work was supported by the U. S. Department of Energy Contract No. EY-76-C-02-3073. Reproduction, translation, publication, use and disposal, in whole or in part, by or for the United States Government is permitted.

Techniques for Measuring the Alpha-Particle Distribution in Magnetically Confined Plasmas

D.E. Post, D.R. Mikkelsen, R.A. Hulse,
L.D. Stewart*, and J.C. Weisheit**
Plasma Physics Laboratory, Princeton University,
Princeton New Jersey 08544

MASTER

ABSTRACT

Methods are proposed for measuring the alpha-particle distribution in magnetically confined fusion plasmas using neutral-atom doping beams, ultraviolet spectroscopy, and neutral particle detectors. In the first method single charge exchange reactions, $A^{o} + He^{++} \rightarrow A^{+} + (He^{+})^{*}$, are used to populate the $n=2$ and $n=3$ levels of He^{+}. The ultraviolet photons from the decaying excited states are Doppler shifted by 5-10 Angstroms from those produced by the thermalized alpha-particle 'ash'. In the second method double charge exchange reactions, $A^{o} + He^{++} \rightarrow A^{++} + He^{o}$, enable fast neutralized alpha-particles to escape from the plasma and be detected by neutral particle analysers. These methods are distinguished from similar techniques of observing plasma impurities in that they allow a determination of the dependence of the distribution function on energy and pitch angle, as well as spatial position. Detector configurations are analyzed, count rates are estimated and their detectability is discussed. A preliminary analysis of the feasibility of the required neutral

DISCLAIMER

beams is presented, and exploratory experiments on existing devices are suggested.

* Exxon Nuclear Co.

** Lawrence Livermore Laboratory

1. INTRODUCTION

Many fusion reactor designs rely on charged fusion product heating of the bulk plasma. The results from neutral beam heating experiments in tokamaks [1] have led to the expectation that the fusion products will behave classically, i.e., the particles will follow guiding-center orbits and interact with the plasma particles through incoherent two-body collisions. Collective phenomena may, however, be important, and both beneficial and deleterious 'anomalous' processes have been theoretically predicted [2-4]. It seems likely that the questions about fusion product interaction with the plasma can be resolved only by experimental means and this is expected to be an important research issue for the first generation of large D-T burning tokamaks (JET and TFTR).

Diagnostic experiments capable of detecting the escaping, charged fusion products [5,6] will provide important information on gross confinement but they cannot be expected to provide much information about the behavior of the confined fusion products. Escaping neutralized fusion products or light emitted by these particles would provide useful information about the confined particle distribution. Unfortunately, the naturally occuring densities of these neutrals and single electron ions appear to be too low to provide detectable signals.

It has long been known that neutral atom 'doping' beams can be used to endow plasma ions with electrons through charge exchange reactions [7]. This provides an effective means of boosting the observable populations in plasmas for both optical [8,9] and neutral particle [10] detection of impurities as well as majority species. Burrell [11] and Suckewer [12] have proposed using doping beams to detect the thermalized ^4He ash from D-T reactions. We are presently concerned with the detection of the fast, non-thermal fusion product distribution, and we shall show that this difference in target population introduces new features which enhance the usefulness of these kinds of detection techniques but increase the technical difficulties.

In this paper we shall consider, in some detail, the detection of the D-T reaction product ^4He, but it should be realized that the general features will be the same for the charged products of other fusion reactions. We shall assess the feasibility of measuring the alpha-particle distribution using neutral doping beams of H, H_2, ^3He, and Li. The reactions which concern us are:

I) $^4He^{++} + H^\circ \rightarrow (^4He^+)^* + H+$

II) $^4He^{++} + H_2{}^\circ \rightarrow (^4He^+)^* + [\ H_2{}^+ \text{ or } p + H^\circ \text{ or } e + 2p\ ]$

III) $^4He^{++} + {}^3He^\circ \rightarrow (^4He^+)^* + [\ {}^3He^+ \text{ or } e + He^{++}\ ]$

IV) $^4He^{++} + Li^\circ \rightarrow (^4He^+)^* + [\ Li^+ \text{ or } e + Li^{++} \text{ or } 2e + Li^{+++}\ ]$

V) $^4He^{++} + H_2{}^\circ \rightarrow {}^4He^\circ + 2p$

VI) $^4He^{++} + {}^3He^\circ \rightarrow {}^4He^\circ + {}^3He^{++}$

VII) $^4He^{++} + Li^\circ \rightarrow {}^4He^\circ + [\ Li^{++} \text{ or } e + Li^{+++}\ ]$

In reactions I through IV the $^4He^+$ will usually be produced in an excited state and the promptly emitted decay photon may be detected. In reactions V through VII there will be decay photons but the $^4He^o$ atoms appear to be more easily detected.

An important characteristic of the cross sections [13,14] (shown in Figure 1) of all these reactions is the sharp cutoff for relative velocities greater than 2-3 x 10^8 cm sec^{-1} (we have been unable to find any cross section data for reaction VII, but we expect it would be similar to the other double charge exchange cross sections). This inhibits the neutrals from interacting with alpha-particles with velocities, $\vec{v}_\alpha$, which do not satisfy

$$v_{rel} = |\vec{v}_\alpha - \vec{v}_{beam}| < v_{cutoff},$$

and this velocity selectivity is the source of the distinguishing features of our proposed detection techniques. The ordering $v_{thermal} < v_{beam} < v_{cutoff}$ was the case in all previous experiments which used doping beams and thus most of the particles in the target populations satisfied the selection criterion.

Since the initial velocity of an alpha-particle is $v_o = (2E_o/m_\alpha)^{1/2} = 13 \times 10^8$ cm sec^{-1}, our velocity ordering is $v_{cutoff} < v_{beam} < v_o$. This ordering necessitates the injection of very fast neutral particles in order to induce charge exchange reactions involving the faster members of the ^4He distribution. The beam energy must be $E_{beam} \sim (A/4)3.5$ Mev - 880 keV/Amu - where A is the atomic weight of the beam particle, and the difficulty of obtaining these high beam energies provides a strong inducement for using

light neutral beam particles. The velocity selecting behaviour of the cross sections makes these reactions very useful probes of the velocity space distribution of alpha-particles. This point is illustrated in Figure 2, where the larger circle delimits the bounds of the alpha-particle distribution in velocity space, and the smaller circle indicates the high velocity cutoff in the cross sections and is centered on the end of the velocity of the doping beam. The ^4He ions which react with the doping beam are primarily those which are close in velocity space to the beam particles, and thus the photons from $(^4He^+)^*$ can be observed with large Doppler shifts and are spectroscopically separable from the thermalized ash emissions. Likewise, the final state $^4He^\circ$ atoms will have large energies which will enable them to easily pass through the plasma before being reionized, and to be readily distinguished from less energetic background particles.

In Section II we present a detailed discussion of the atomic processes involved in the penetration of the doping beam, the charge exchange reactions, radiative decay of the excited $^4He^+$, and reionization of $^4He^+$ and $^4He^\circ$, together with UV spectral line shapes and velocity distributions for the escaping $^4He^\circ$. This is followed, in Section III, by an outline of the beam-plasma-detector geometry and estimated count rates for all of the reactions, plus a preliminary indication of the most promising beam-detector combinations. An assesment of the required neutral beam technology is provided in Section IV, and some preliminary experiments on existing devices are suggested in Section V.

2. ATOMIC PROCESSES

We begin this Section by determining the practicable range of particle energies for the neutral doping beams. Then we evaluate expressions for $\langle\sigma v\rangle$ and $d\langle\sigma v\rangle/d\Omega$ using classical and non-classical alpha-particle distribution functions, and the resulting UV line shapes and escaping neutral particle velocity distributions are presented. The ionization rates of the $^4He^+$ and $^4He^\circ$ are estimated, and we find that reionization of the higher excitation levels is likely.

The upper limit on the desired neutral beam particle energy has been given above as 880 keV/Amu. The lower limit is set by the necessity that the beam penetrate to the center of the plasma. We require that the 'ionization depth' to the center of the plasma, $1 = \int n d\ell$, be no greater than one. Ions provide the dominant source of ionization so we have determined the lower limit on E_{beam} for penetration of TFTR from $1 = \int n d\ell = \sigma\ 1x10^{16}\ cm^{-2}$ or $\sigma = 1x10^{-16}\ cm^2$. The ionization cross sections are taken from Freeman and Jones [15] and Shipsey, et al. [14], and the full range of useful beam energies is given in Table I for each beam species.

In estimating the reaction rates in the next Section, we shall use the quantity

$$1) \quad \langle \sigma v \rangle = \int f^*(\vec{v})(\vec{v} - \vec{v}_{beam})\sigma(\vec{v} - \vec{v}_{beam})d^3v$$

where $f^*(\vec{v})$ is the velocity-space alpha-particle distribution function (normalized to unity). The reaction rate density is then $R=n_{beam}n_\alpha\langle\sigma v\rangle$ where n_{beam} and n_α are the beam and alpha-particle densities. In magnetic confinement devices one expects $f(\vec{v})$ to be cylindrically symmetric about the local magnetic field direction, thus allowing it to be expressed as $f(v,\theta)$ in a suitably oriented spherical coordinate system. The result for $\langle\sigma v\rangle$ is therefore a function not only of v_{beam} but also of the angle, θ_{beam}, between $\vec{v}_{beam}$ and $\vec{B}$. Within the limits set by physical constraints on the beam injection angle and detector configurations, it should be possible to determine the dependence of f on both v and θ.

In what follows we assume an isotropic form for the alpha distribution function, f=f(v), even though the real distribution may have anisotropies caused by the anisotropic source from beam-target and beam-beam fusion reactions, loss-cones, and finite-width orbit effects. These complexities are beyond the scope of this preliminary analysis. We expect any large-scale angular features in f(v) to be reflected in $\langle\sigma v\rangle$, and the existence of broad loss-cones (> 30 degrees wide) should also be noticeable.

In our evaluation of $\langle\sigma v\rangle$ we use two alpha-particle distributions, one being that produced by the classical binary-collision process, and the other being a non-classical form that is intended to provide a qualitatively different distribution with which we can illustrate the sensitivity of different observables to the form of f(v). The classical distribution is obtained from the usual Fokker-Planck equation [16] (in isotropic form):

$$2)\quad \frac{df(v)}{dt} = (v^2\tau_{se})^{-1}\ \frac{d}{dv}\ [(v^3+v^3_c)f(v)] \ +\ S(v)$$

where $\tau_{se}^{-1}=(8/3)(\pi m_e/2)^{1/2}(e^4 \ln\Lambda_e n_e)/(m_p(kT_e)^{3/2})$

and $v_c=[(3/4)(\pi m_p/m_e)^{1/2}(\sum_i Z_i^2 n_i/A_i n_e))(\ln\Lambda_i/\ln\Lambda_e)]^{1/3}(2kT_e/m_p)^{1/2}$.

The steady state distribution is given by

$$3)\quad f(v) = [\tau_{se}/(v^3 + v_c^3)]\int_v^\infty S(u)u^2du$$

If we approximate the source by a delta function,

$$S(v) = R_\alpha \delta(v - v_o)/v_o^2,$$

then the distribution is simply

$$f(v) = \tau_{se}R_\alpha/(v^3 + v_c^3) \quad v < v_o, \quad 0 \text{ otherwise.}$$

Integrating over v we get the density of alpha-particles:

$$\begin{aligned} n_\alpha &= \int f(v)v^2dv \\ &= (\tau_{se}R_\alpha/3)\ln[1 + (v_o/v_c)^{1.5}] \\ &= \tau_s R_\alpha \end{aligned}$$

where τ_s is the slowing down time.

In our calculations we have used a more realistic source term of the form

$$4)\quad S(v) = (R_\alpha/\delta v_o\sqrt{\pi})e^{-[(v - v_o)/\delta v_o]^2}$$

where $\delta = \Delta E_o/2E_o$, and ΔE_o is the Gaussian width of the alpha-particle initial energy distribution. This is appropriate for both thermonuclear [17] and beam-target [18] processes. By integrating over v, we obtain the alpha-particle production rate,

$$R_\alpha = n_T(n_D\langle\sigma v\rangle_{th} + n_{beam}\langle\sigma v\rangle_{bt} + n_{beam}\langle\sigma v\rangle_{bb}),$$

where the terms on the right are the thermonuclear, beam target, and beam-beam contributions. During the steady state phase of a beam-driven tokamak discharge the thermonuclear term is comparable to the beam terms, and thus it provides a convenient estimate of the production rate.

Plasma parameters which are typical of the anticipated performance of TFTR are given in Table II. With these conditions we have used Eqs. (3) and (4) to calculate the classical alpha-particle distribution that is shown in Figure 3. Variation of the plasma parameters by factors of 2 or less do not cause any qualitative changes in the shape of the classical distribution.

Sigmar and Chan [4] have suggested that wave-particle interactions may produce rapid, diffusive loss of fast alpha-particles. This loss prevents the buildup of the low energy part of the alpha distribution with the result that the alphas continue to drive the waves. For illustrative purposes we shall use an ad-hoc "non-classical" distribution

$$f^*_{nc}(v) = f^*_{cl}(v)\,(v/v_o)^4$$

(see Figure 3) to explore the effect of such an anomalous loss on the optical line profiles and $^4He^o$ velocity distributions. It is intended that this distribution model a process which removes alpha-particles after they have diffused to the limiter or wall: very few high-energy particles have diffused sufficiently to be lost, and very few low-energy particles have mananged to remain confined to the plasma region. By not renormalizing $f^*_{nc}(v)$ but requiring instead that $f^*_{nc}(v_o)=f^*_{cl}(v_o)$ we may scale the two distributions by the same alpha-particle density, n_α.

The classical and non-classical distributions were used to evaluate Eq.(1) and the results are presented in Figure 4. The general behavior of the $\langle\sigma v\rangle$ qualitatively follows the shape of the distribution functions. Note that even though $f^*_{nc}(v_o)=f^*_{cl}(v_o)$ we find that $\langle\sigma v\rangle_{nc} < \langle\sigma v\rangle_{cl}$; this is so because $\langle\sigma v\rangle$ samples $f^*(v)$ over a range of velocities and most of the contribution to the integral comes from $v=v_o-v_{cutoff}$ where $f^*_{nc} < f^*_{cl}$. The integral nature of $\langle\sigma v\rangle$ leads to a local averaging of $f(v)$ which is easily seen in the very gradual fall of $\langle\sigma v\rangle$ near $v=v_o$; the averaging is

least pronounced in reaction IV, which has the smallest cutoff velocity.

While photons will be emitted isotropically after reactions I-IV, the neutralized alpha-particles in reactions V-VII will escape in the general direction of the neutral beam. All the charge exchange reactions are strongly forward-peaked in the C-M frame, so the velocity of the $^4He^{++}$ will be unchanged by the double charge exchange and the differential $\langle\sigma v\rangle$ for reactions V-VII is

$$\frac{d\langle\sigma v\rangle(\theta)}{d\Omega} = \int f^*(v)\, v_{rel}\sigma(v_{rel})\, v^2 dv \qquad 5)$$

where $v_{rel} = [v^2 + v^2_{beam} - 2vv_{beam}\cos(\theta_{beam})]^{1/2}$

This has been calculated as a function of θ_{beam} for several values of v_{beam} and the results are plotted in Figure 5. The high velocity cutoff in the cross sections is responsible for the utoff in the differential $\langle\sigma v\rangle$ at large angles. Since the cutoff angle is roughly proportional to v_{cutoff}/v_{beam}, it is larger for smaller beam velocities.

The fact that the alpha-particle velocities are virtually unchanged by the charge exchange event, together with the very short lifetimes of the excited states, permits us to equate the initial velocity of $^4He^{++}$ to the velocity of the excited $^4He^+$ in reactions I-IV. This makes the calculation of the expected line shapes s raightforward, and these profiles are presented in Figure 6 for a detector with a line-of-sight along the beam axis. We have assumed that the mix of excited states in $^4He^+$ is independent of v_{rel} since the relevant cross sections are not available. The

Doppler shifts are quite large (5-10 Angstroms) and the lines are rather broad, those reactions with smaller cutoff velocities producing sharper lines. The profiles generally are assymetric and quite strongly displaced from the Doppler shift corresponding to the doping beam velocity. These effects are due, of course, to the strong gradients in both of our trial alpha-particle distribution functions. This point is important for it means that even with a fixed beam velocity it is possible to determine whether f(v) is an increasing or decreasing function of v.

The $^4He^o$ velocity distributions of reactions V-VII are the neutral particle analogues to the UV line shapes of reactions I-IV. The distribution of emerging neutrals is given by the integrand of Eq.(5). A typical set of distributions is shown in Figure 7 for a beam-detector angle of 20°. Again we note the asymmetry and the displacement of the peaks, with the opposing gradients of the classical and non-classical alpha distributions producing displacements of opposite sign. While these results are quite similar to the UV line shapes, the $^4He^o$ distributions differ in one qualitative way: for low values of θ and v_{beam} the curves have a double peak structure. This arises from the fact that at each angle, θ, all emerging neutrals of a given speed, v_α, have the same velocity relative to the beam particles, i.e.

$$v_{rel} = [v_\alpha^2 + v^2_{beam} - 2v_\alpha v_{beam}\cos(\theta)]^{1/2}.$$

As v_α varies from 0 to ∞ the relative velocity decreases to the minimum relative velocity, $v_{min}=v_{beam}\sin(\theta)$, and then increases without limit. If v_{min} is small enough, the quanity $v_{rel}\sigma(v_{rel})$ will be maximized for some $v_{rel} > v_{min}$ and thus as v_α increases $v_{rel}\sigma(v_{rel})$ will

achieve its maximum twice. This is in strong contrast to the UV photon case where particles with differing v_{rel} may contribute to the signal at a given wavelength and the spectral lines always have a single peak.

To complete our discussion of the relevant atomic processes at work in the plasma we now examine the distribution of electronic states in the $^4He^+$ and $^4He^0$ produced by the charge exchange reactions, and compare the time scales of the radiative decay and reionization processes. In three of the reactions considered there is a resonant final state for the $^4He^+$ or $^4He^0$ (see Table I). When the relative velocity in these reactions is small ($v < 10^8$ cm sec^{-1}) one would expect most of the captured electrons to be found in the resonant states; but if the relative velocity is large ($v > 3x10^8$ cm sec^{-1}) or there is no resonant state, the electrons might be distributed among a number of levels [14,19]. A broad distribution of final states is undesirable in two ways: i) the photons from $(^4He+)^*$ will be dispersed to a number of lines rather than being concentrated in a single line, and ii) ionization cross sections rise as the excitation level increases and this causes a loss of signal due to prompt reionization. The first problem is mitigated by the fact that in charge exchange reactions one expects high ℓ states to be preferred over the low ℓ states of the same level n, so the $\Delta\ell=1$ selection rule will force a significant fraction of the electrons in the n=3,4, and 5 levels to cascade through the 2p->1s transition.

In order to assess the importance of reionization and reexcitation of the $^4He^\circ$ and $^4He^+$ we have used Jacobs' [20] theoretical cross sections which are based on Born approximations applied to one-electron systems. We expect this model to be applicable to the excited states of He° because the excited electron is responsible for most of the total ionization cross section and, since it is 'outside' the 1s electron, we expect that it will behave as if it were bound in an H atom; this line of reasoning is supported by the close correlation in the energy levels of the excited states of H and He. We do not consider doubly excited states of He because they are promptly autoionizing and they will not contribute to our signal in the experimentally measured cross sections we are using. At large velocities the proton and electron ionization cross sections are identical and, since the cross sections fall as $1/v^2$, the protons are the dominant cause of ionization.

The $^4He^\circ$ must pass through a column density of 10^{16} cm^{-2} to get to the neutral particle analyzers, and this is a serious obstacle for low energy particles. The sum of the ionization and charge exchange cross sections for $He(1s^2)$ is greater than 10^{-16} cm^2 for velocities less than 5×10^8 cm sec^{-1} (500 keV ^4He) so we shall take that to be the lower limit on the velocity of the escaping $^4He^\circ$. The reionization rates (for $n_i = 10^{14}$ cm^{-3}) of excited states of He^+ and He° at this velocity are given in Table III together with the radiative decay rates [21]. Since the ionization rates are lower at higher speeds this is a worst case

analysis. We find that only the singlet ($1s2p$) and ($1s3p$) states of He° will decay to the relatively safe ($1s^2$) level; other states must be collisionally converted to these states to avoid reionization.

In the case of He^{+} we find that electrons in the 2p a l states will survive to cascade through the 2p -> 1s (304 Angstroms) transition as will roughly half of the electrons in the 4f state. The 3p -> 1s (256 Angstroms) transition is faster than reionization but most electrons in the 4d state will not contribute to this line. Again, collisions may allow some fraction of the electrons in other 2ℓ and 3ℓ states to pass through the desired transitions. Excitation cross sections are approximately the size of the ionization cross sections so reexcitation will neither increase the photon signals nor reduce the He° signal by repeatedly raising the electrons to higher states.

It is now clear that details of the alpha-particle distribution can be observed by employing neutral beams to enhance the populations of fast $^4He^{+}$ and $^4He^{\circ}$. The velocity-space selectivity of the charge exchange process is demonstrated by the qualitative similarity between the forms of $f(v)$ and $\langle\sigma v\rangle(v_{beam})$ in Figures 3 and 4, respectively. Even with observations at only one beam energy, it is possible to distinguish between the classical and non-classical alpha-particle distributions by measuring the velocity distributions of the $^4He^{+}$ and $^4He^{\circ}$.

3. DETECTION SCHEMES

We can construct a simple model for the interaction volume between the beam and alpha-particles to provide estimates of signal strengths for various detection geometries. Our beam and detector arrangement is illustrated schematically in Figure 8; the actual situation on any specific machine will depend on port locations, coil obstructions, etc., but the general trends will be the same. The beam is modeled as a long square box with sides of width d (see Figure 9). The detector sees everything in a long box with sides of width s. The detector is located at a distance λ from the center of the interaction volume. The alpha density is taken to be constant out to r=.5a, and thus the length of the interaction volume is the smaller of $2(aR)^{1/2}$ or $s/sin(\theta)$, where θ is the angle between the beam and detector axes. Assuming typical TFTR parameters (a=85 cm, R=250 cm, and λ=500 cm), and hypothetical detector and beam parameters (s=10 cm, d=7 cm), we can compute the interaction volume as a function of θ. We can also compute a factor δ, shown in Figure 10, which converts the volume source rate P_ν to a fluence at a detector ($\Gamma=\delta P_\nu$). The interaction volume varies from 1.3×10^4 cm^3 to 1.4×10^3 cm^3 as θ varies from 0° to 20°. Two conversion factors can be defined, $\delta_{4\pi}$ for the case where the emission is isotropic and $\langle\sigma v\rangle$ is defined in cm^3 sec^{-1}, and δ for the case where the emission is anistropic and $\langle\sigma v\rangle$ is defined in cm^3 sec^{-1} $steradian^{-1}$. The scaling for isotropic sources is $\Gamma=P_\nu d^2 s/(\sin(\theta) 4\pi\lambda^2)$ for $\theta > 2°$ assuming $s > d$. Table IV lists the

expected fluence levels at the detector assuming $n_\alpha = 10^{12}$ cm^{-3} and $n_{beam} = 10^8$ cm^{-3} for the H$^\circ$ beam and 10^5 cm^{-3} for the other beams. The other beams are more difficult to construct, and a density of $\sim 10^5$ cm^{-3} is used as a criterion for the beam to be of interest. The estimate of $\sim 10^{12}$ cm^{-3} for n_α comes from bulk considerations of Q=1 for TFTR with 24 MW of heating where the alphas are largely within r=30 cm and τ_s =400 msec. The TFTR charge exchange detectors are expected to work with fluences of $\sim 10^4$ cm^{-2} sec^{-1} for protons in the 20-100 kev range with a 5 kev resolution [22]. If these alphas can be counted efficiently, this translates to a minimum helium beam density of 2×10^3 cm^{-3} to provide 10^4 cm^{-2} sec^{-1} from a ^{3}He$^\circ$ beam. If we allow another factor of 10 to be able to work with Q=0.1 ($n_\alpha \sim 10^{11}$ cm^{-3} instead of 10^{12} cm^{-3}) experiments, and a factor of 5 to account for other effects such as beam attenuation, ionization of excited states of ^{4}He, etc., one obtains a rough estimate of $\sim 10^5$ cm^{-3} for a minimum beam density. The $\langle\sigma v\rangle$ for reactions I-IV rises as E_{beam} decreases so detectable signals at E_{beam}=880 keV/nucleon imply that lower energies will also be detectable if the slowing down is classical. The $d\langle\sigma v\rangle/d\Omega$ for reactions V and VI at ten degrees is not as strong a function of E_{beam}; $d\langle\sigma v\rangle/d\Omega$ just becomes broader in angle as v_{beam} drops.

The peak photon production rates are on the order of 10^{11} cm^{-3} sec^{-1} for the H^{o} beam and 10^{8} cm^{-3} sec^{-1} for the other beams. Presuming an observable path length of from 10cm to 100 cm through the beam interaction region, an emission rate of ~ 10^{11} photons cm^{-3} s^{-1} near 300 Angstroms is one to two orders of magnitude below that which can be straightforwardly observed in current tokamak plasmas. The detection sensitivity of such observations is in principle determined by some combination of instrumental limitations (such as scattered light in the spectrometer) plus the magnitude and fluctuation spectrum of background line and continuum emission from the plasma. For a $n_e = 10^{14}$ cm^{-3}, 10 kev plasma bremsstrahlung in the 4 Angstrom bandwidth of the expected $^4He^+$ emission line is approximately 10^{11} photons cm^{-3} s^{-1}. Bremsstrahlung alone is thus not a limiting factor in the current observations, nor should it be a serious problem for detection of the $^4He^+$ line emission. Beyond this conclusion, however, current observational experience is not sufficient to clearly identify the relative importance of the other potentially limiting factors present. It is therefore not possible to predict with confidence the ultimate sensitivity achievable through instrumental improvements or by additional techniques such as modulation of the diagnostic beam in order to reduce the effects of fluctuation noise from the plasma background emission. There does not, however, seem to be any prima facie reason why the required sensitivity could not be reached. Exploratory observations and experimentation with exisiting equipment is necessary to determine if the detection and measurement of the relevant line emission from these alpha-particle

detection techniques is practical in a realistic tokamak environment.

Table IV also lists neutral alpha fluences, which give, at θ=10 degrees, fluences of ~ 4 x 10^5 cm^{-2} sec^{-1} at a detector 5 meters from the plasma. This fluence level for 50 keV protons is measureable with current charge exchange analyzer systems. These analyzers detect high energy neutral protons by stripping them in helium gas cells, selecting e/m by magnetic and electrostatic analyzers, and counting particles with electron multipliers. The fields required to analyze a 3.5 MeV $^4He^{++}$ are< 5 kG for a 50 cm radial analyzer. The design of an analyzer is straightforward and could even involve only modifications of existing charge exchange analyzers. Current charge exchange analyzers use a stripping cell of helium or hydrogen. At 10-100 keV for H^o, the stripping cross section is ~ 10^{-16} cm^2 [23]. The density in the cell is ~ 1 millitorr or ~ 10^{14} cm^{-3}. This gives a mean free path of 100 cm, which for a 10 cm length cell implies that ~ 10% of the neutrals are stripped. At 3.5 MeV, the cross section for singly ionizing $^4He^o$ with a H_2 gas cell is 3.4x10^{-17} cm^2 [23]. For a density of 10^{14} cm^{-3}, this implies a mean free path of 300 cm. A 65 cm long gas cell, shielded from the magnetic field, would strip ~ 20% of the $^4He^o$ to $^4He^+$. The cross section for the ionization of the $^4He^+$ in the cell is ~ 5x10^{-17} cm^2, so the $^4He^{++}$ fraction would be small. Very little of the $^4He^+$ would be converted back to $^4He^o$ since the charge exchange $^4He^+ + H^o \rightarrow {}^4He^o + p$ has a cross section < 10^{-19} cm^2 at 3.5 MeV. Thus gas stripping cells could be operated with H_2

for the neutral alphas with efficiencies comparable to the efficiencies achieved in present neutral hydrogen analyzers.

There will be a small neutral helium flux from the atomic hydrogen beam due to two successive single charge exchanges, $^4He^{++} + H^o \rightarrow {}^4He^+ + H^+$, and $^4He^+ + H^o \rightarrow {}^4He^o + H^+$. The cross section [13] for this second reaction is ~ 10^{-16} cm^2. A crude estimate of the volume production rate using reference parameters is $n^2_{beam} n_\alpha \langle\sigma v\rangle(cxHe^{++},H^o)\langle\sigma v\rangle(cxHe^+,H^o)\tau_c$, where τ_c is the confinement time of the $^4He^+$ in the beam path. For a tangential beam with $v_{parallel} \sim v$, $\tau_c \sim Rd/v \sim 3x10^{-8}$ sec for TFTR. This yields a production rate of $2x10^4$ cm^{-3} sec^{-1}, which is probably too small to be detectable and is much lower than the rate from the double charge exchange reactions.

The high energies of the neutral alphas makes stripping foils attractive. The foils dispense with the complexities of pumping and shielding systems of gas cell strippers. The efficiency of $^4He^{++}$ production is over 95% at 3.5 MeV, and over 80% at 1 MeV. The stopping power for iron foils, -dE/dx, is 450 keV/micron [24]. Iron foils are available in thicknesses as thin as 200 Angstroms, so the energy loss in the foil could be as low as 10 keV. Heat loading on such foils may be a problem since they will have a vacuum line of sight to the plasma. If TFTR radiates ~ 20 MW, then the heat flux 7 meters away from the center of the torus is ~ 3 watts cm^{-2}, which must be borne by the foil. These heat loads could be tolerated by foils supported on a wire mesh of a highly

conductive metal. The overall efficiency of such a foil stripper could still be ~ 90%. The optimum choice of foils would involve tradeoffs of minimum angular scatter and energy loss, and maximum strength, life, and thermal load capacity.

The neutron background in an experiment such as TFTR would be ~ 10^{12} cm^{-2} sec^{-1} at a detector 7 m from the center of the torus. This flux will need shielding, but would need no more shielding than that planned for the current TFTR charge exchange analyzer designs. Solid state detectors with good energy resolution might become feasible if the gamma and neutron background could be significantly reduced. These detectors offer the advantage of energy resolution, high count rates, simple design, and high efficiency. It might even be possible to dispense with energy and mass analysis with magnetic and electric fields with such detectors.

Detection of the direct recombination photons from $(^4He^+)^*$ would be difficult. It will require significant spectrometer improvements, and possibly the use of beam modulation, long integration times, etc., to extract a signal from the background. Detection of the neutral ^4He (3.5 MeV) is feasible with current technology. Either gas stripping cells, or stripping foils could be used to produce $^4He^+$ or $^4He^{++}$, which could be analyzed with either current instruments, or modest extensions of current instruments. The background and noise problems faced are no more

severe than those faced by analysis of the charge exchanged proton flux from fusion plasmas in TFTR.

4. NEUTRAL BEAM FORMATION

4.1 General Considerations

Formation of neutral H, H_2, ^3He, and Li beams with 0.9 MeV per nucleon was considered. Because the desired combinations of energy, beam particle flux, and beam size are beyond existing technology, projections were made of attainable beam current densities and other beam technologies. In most cases, extrapolations were also required for cross sections or neutralization efficiencies at 0.9 MeV per nucleon [23,25-32]. A transmission loss of 50%, corresponding to emittances of 1-2 x 10^{-2} cm rad $MeV^{1/2}$ for a TFTR-like geometry, was assigned. The resulting estimates of attainable beam density are listed in Table V for each of the various beam production methods considered. Also given in Table V are the neutralization efficiencies, and the accelerator power and current required to supply 50 cm^2 of beam. For the beams to be used for double charge exchange, the accelerator requirements are based on an upper limit to the beam density of 10^5 cm^{-3}. Although this beam density may be considered a minimum for detectable signals (see section III), the accelerators will require significant development beyond

state-of-the-art in every case. Production of 0.9 MeV H^o, 1.8 MeV H_2^o, 2.6 MeV $^3He^o$ and 6 MeV Li^o are now considered individually.

4.2 0.9 MeV H^o

Because of the low neutralization efficiency, brute force acceleration of H^+ yields unacceptably low beam densities. Considering an H^- source yields an estimated 4×10^8 cm^{-3}, but at 0.9 MeV this is an average beam power density of 60 kW cm^{-2}. Reducing the average beam power density to a more technologically manageable 10 kW cm^{-2} results in a beam density of 6×10^7 cm^{-3}, and the corresponding accelerator requirements are 1 A and 1 MW. If the lower beam density is acceptable, this alternative is attractive because it is a relatively small extrapolation from existing technology, because the development required is already a part of the existing neutral beam development program [33] and because the 0.9 MeV neutral fractions have been measured [27].

4.3 1.8 MeV H_2^o

The production of H_2^o is difficult because the cross sections for formation of H_2^o are small compared with the competing break-up and ionization cross sections. Thin neutralizers yield optimum H_2^o production efficiencies, but these are calculated to be only $1\text{-}2 \times 10^{-4}$, and the resulting beam densities are $2\text{-}4 \times 10^4$ cm^{-3}. Accelerator requirements of 4 A and 7-10 MW are three orders of magnitude larger than has been achieved at this energy.

4.4 2.6 MeV $^3He^0$

$^3He^+$ acceleration leads to an estimated beam density of 10^5 cm^{-3}, but the accelerator requirements are very ambitious: 1.5 A and 3.5 MW. Starting with 3.5 Mev $^3HeH^+$ and using an optimized cell thickness improves the predicted production efficiency and reduces the accelerator requirements to ~ 150 mA and 0.5 MW. This is still two orders of magnitude higher than has been achieved.

A promising approach is the conversion of 20 keV $^3He^+$ to $^3He^-$ in a Na or Li cell, followed by acceleration to 2.6 MeV and neutralization. The accelerator requirements, 5 mA and 15 kW, (plus 35 kW across 20 kV) is a reasonable extrapolation from existing accelerators. We note, however that this is a two order of magnitude extrapolation of total He^- current.

4.5 6 MeV Li^0

Positive ion acceleration again leads to low beam densities and extreme accelerator requirements. For Li^-, an assumed source current density of 10 mA cm^{-2} and an assumed neutralization efficiency of 0.5 results in a relatively low 4 mA requirement. However, the 6 Mev is higher than has been achieved in a long-pulse accelerator at any current, and development within 5 years would be difficult.

5. EXPERIMENTAL AND THEORETICAL SUPPORT AND ADDITIONAL APPLICATIONS

It may be useful to try parts of the ideas presented above on present or future machines short of TFTR, JET, or ETF. Difficulties with such preliminary proof of principle experiments are that experiments before TFTR and JET will have few fusion products to detect, and high energy, high current beams are not yet available.

Nevertheless there are a few facets of the scheme that could be tested on a device like PDX, which has a flexible, high energy diagnostic neutral beam (FIDE) and high power neutral beam heating(6-8MW). One such test would be measurement of the 304 Angstrom light from excited $^4He^+$ formed by injecting 50 keV neutral beams into a ^4He plasma. The primary PDX beams will have a density of $\sim 2x10^9$ cm^{-3}. The diagnostic beam density will be smaller. With a helium density of $5x10^{13}$ cm^{-3}, this gives a photon production rate in the beam path of $n_{beam}n_{He}\langle\sigma v\rangle \sim 2x10^{16}$ cm^{-3} sec^{-1}. This emission might be detectable. The helium will recycle and recombine at the plasma edge and thus produce some $(He^+)^*$, which could complicate the experiment. Degrading the emission rate by reducing the helium density, or the beam current, allows exploration of the limits of detectable signals. A detailed measurement of the noise spectrum in a real experiment around 304 Angstroms would allow a realistic assessment of the need for and efficacy of possible noise reduction techniques. The flexible diagnostic neutral beam (FIDE) on PDX could be modified if beam

modulation was a promising approach. Since such experiments have already been suggested by Burrell [11] and Suckewer [12], it is likely that some of the needed information will become available in 1980 or 1981. A significant effort to improve the noise levels and sensitivities of spectrometers sensitive to 300 Angstrom photons would also be useful.

Adding He pumping capability to one of the primary beams or a diagnostic doping beam for use on PDX with a helium plasma would allow the formation of helium neutrals generated by double charge exchange of the hot central thermal $^4He^{++}$ and the neutral helium beam. Thus detection of the high energy tail of the ^4He neutrals (similar to T_i measurements using hydrogen charge exhange) would suggest that $^3He^o + {}^4He^{++} \rightarrow {}^3He^{++} + {}^4He^o$ scheme would work if the beams could be built. Detection of 5-20 keV $^4He^o$ poses a slightly different problem than detection of 3.5MeV $^4He^o$, however.

Another possibility closer to alpha detection is to use a moderate energy $^4He^o$ beam (as high a current and energy as available) to look for the 800 keV $^3He^{++}$ from D-D reactions during high power D injection into D plasmas on PDX or other machines. Estimates of the neutron production on PDX indicate that $n_{^3He^{++}} \sim 10^8$ cm^{-3} (assuming I= 500 kA, $\tau_s \sim 100$ msec, and $dN/dt \sim 10^{16}$ neutrons sec^{-1} during injection). The count rates would be lower than on a D-T experiment, but the noise problems would be lower also, and helium beams of 500-1000 keV could be used here. The same sort of detectors as needed for 3.5 MeV $^4He^o$ could

be tested. The production rate might be as high as $n_{^3He^{++}} n_{beam} \langle \sigma v \rangle \sim 10^7$ cm^{-3} sec^{-1}, which would probably be detectable. The measurement could be correlated with the 14 MeV neutron signals from the slowing down T reacting with the background D.

The feasiblility and utility of each of these "proof of principle" measurements will need to be worked out in detail for any experiment on which they might be tried. However, these preliminary measurements would provide "milestones" for the alpha measurement on a D-T experiment. The beam development could proceed independently of intermediate experiments on tokamaks since it is a well defined, independent project.

Use of charge exchange to measure alpha-particles would benefit from additional atomic physics experiments and theoretical work. The single and double charge exchange cross sections of neutral lithium with alphas have not been measured. It would be a relatively straightforward experiment, and should be done if the prospects for making Li^o beams improve. All of the relevant cross sections have uncertainties, some as large as a factor of two, and improvements in the accuracy of the cross sections would increase the usefulness of the alpha diagnostic. The cross section for reaction I should be extended to an interaction energy of $E_{4_{He}} = 3$ MeV.

An examination of the single and double charge exchange cross sections [13] for neutral atoms and $^4He^{++}$ indicate that neutral beams of many elements (at least through lead) have single charge exchange cross sections on the order of 10^{-15} cm^2, and many elements from helium at least up through lead have double charge exchange cross sections of ~ 10^{-16} cm^2. Potassium, for example, has peak cross sections of $4x10^{-14}$ cm^2 and $5x10^{-15}$ cm^2, respectively. All of the cross sections fall rapidly for $v_{rel} > 3x10^8$ cm sec^{-1}. Thus even neutral lead beams with $v_{beam} \sim 13x10^8$ cm sec^{-1} could be used to measure the alpha density. However, the large energy required to achieve such a velocity - 880 keV/Amu - strongly favors the use of light atom beams (potassium, for example, would require a 32 MeV beam).

Further work on the cross sections for populating the upper levels of $^4He^o$ and $^4He^+$, the electron cascade paths, and the ionization rates for the excited states is needed to determine whether the UV photons will be concentrated in a few lines and whether reionization will cause serious losses. Much of the work to date in this area has been done in connection with X-ray lasers, and many of the techniques and calculations would undoubtedly apply.

Many of the cross sections relevant to the beam technology assessment are poorly known and should be measured. These measurements should be done soon since they could have an impact on the choice of the primary beam ion and the neutral beam design.

The beam considerations discussed in Section IV rely mostly on extrapolations of existing measurements. The cross sections and neutral fractions for the promising 2.6 MeV $^3He^-$ -> 2.6 MeV $^3He^\circ$ case should be measured. A program for assessing the feasibility of, and then achieving, 5 mA of 20 keV $^3He^-$ could be undertaken prior to and independent of the more expensive high voltage accelerator development. For another interesting case, 0.9 MeV H^- -> 0.9 Mev H°, the existing negative ion beam development program should be supported and made aware of this need.

The proposed technique of using single and double charge exchange of diagnostic neutral beams with fusion reaction products would work for D-D fusion reactors as well. The reaction products of D-D are 1.01 MeV T^+, 3.03 MeV H^+, 820 keV $^3He^{++}$, 3.52 MeV $^4He^{++}$, 3.67 MeV $^4He^{++}$, and 14.67 MeV H^+. Neutral hydrogen beams of suitable energies could detect the H+ and T+ by single charge exchange and analysis of the high energy neutral. D° beams could be used for the H^+ and H° and D° beams could be used for the T^+. Helium beams could be used for all the products (single and double charge exchange). The same general discussion given in Section I-IV would apply with suitable minor modifications.

6. CONCLUSION

We have described two techniques for measuring the alpha-particle distribution in a magnetically confined, D-T plasma. The expected signal strengths have been calculated, and the feasibility of each technique has been estimated.

The first technique is the measurement of the direct recombination radiation from $(^4He^+)^*$, and the second is the detection of high energy neutral $^4He^\circ$ atoms. Both $(^4He^+)^*$ and $^4He^\circ$ are produced by charge exchange with a high energy neutral beam. By varying the beam energy, both techniques allow one to measure the alpha particle distribution function sufficiently accurately to determine if the alpha velocity distribution is strongly non-classical. By varying the beam angle and position the pitch angle and radial distribution of the alphas can be measured.

The techniques were explored in detail for a tokamak (TFTR) because it is likely to be one of the first D-T magnetic fusion experiments. However, the techniques will work for all magnetically confined plasmas, such as mirrors or spheromaks.

The measurement of the UV radiation from $(^4He^+)^*$ will be difficult. It will require significant spectrometer development, and may require long integration times (implying poor time resolution) and modulation of the beam. The second technique, measurement of $^4He^\circ$, has the advantage of a much lower background

(there is no equivalent of bremsstrahlung or impurity emission) since the $^4He^o$ (3.5MeV) is a unique particle. It can be counted and analyzed with high efficiencies. The preliminary estimates presented above indicate that the predicted fluence is greater than the expected detector thresholds for the hydrogen analyzers on TFTR. Factoring in the beam feasibility, a 2.6 MeV $^3He^o$ beam is the most promising candidate. Development of a 5-10 mA, 2.6 MeV $^3He^o$ beam will not be trivial, but should be possible.

The techniques we have described are expensive and difficult, but, at present, there are few other proposals for directly measuring the central alpha-particle distribution. Given the expense of ETF ($\sim \$ 10^9$), $\sim \$ 10^6 - \$ 10^7$ to develop and build a diagnostic to measure the raison d'etre for fusion is not excessive. If development is started now, the beams and detectors could be ready for ETF (1990) and possibly ready for TFTR upgrades (1985).

ACKNOWLEDGEMENTS

The authors gratefully acknowledge encouragement and useful discussions with Drs. Klaus Berkner, Keith Burrell, Joe Cecchi, Harold Eubank, Raymond Fonck, Charles Goldie, Robert Goldston, Richard Hawryluk, Gary McCracken, Sid Medley, Ron Phaneuf, Ken Purser, John Schmidt, Steven Seiler, Eric Silver, Cliff Singer, and Kenneth Young. We are particularly grateful to the authors of references [13] *and* [23] for extremely convenient and useful

compilations of atomic cross sections. The work was performed under DoE Contract No.EY-76-C-02-3073.

REFERENCES

[1] Goldston,R.J., Nucl. Fusion 15 (1975) 651

[2] Lominadze,D.G., Mikhajlovskij,A.B., and Tang,W.M., Sov. J. Plasma Phys. 2 (1976) 286

[3] Bhadra,D.K., General Atomic Report A14729 (1977)

[4] Sigmar,D.J., and Chan,H.C., Nucl. Fusion 18 (1978) 1569

[5] Seiler,S.W., and Hendel,H.W., Bull. Am. Phys. Soc. 23 (1978) 881

[6] Foote,J.H., Lawrence Livermore Lab. report UCRL-81927 (1978)

[7] Kudryatsev,A.M., and Sorokin,A.F., J.E.T.P. Lett. 18 (1973) 286. Afrosimov,V.V., Petrov,M.P., Sadovnikov,V.A., and Ioffe,A.F., J.E.T.P. Lett. 18 (1973) 300.

[8] Isler,R.C., Phys. Rev. Lett. 38 (1977) 1359

[9] Drake,R.P., and Moos,H.W., Bull. Am. Phys. Soc. 24 (1979) 767

[10] Brusati,M., Davis,S.L., Eubank,H.P., Moriette,P., Smith,R.R., and Goldston,R.J., Bull. Am. Phys. Soc. 22 (1977) 1076

[11] Burrell,K.H., Bull. Am. Phys. Soc. 24 (1979) 767

[12] Suckever,S., private communication (1979)

[13] Okuno,K., Charge Changing Cross Sections for Heavy Particle Collisions in the Energy Range from 0.1 eV to 10 MeV: I. Incidence of He, Li, Be, B, and Their Ions, Nagoya University report IPPJ-AM-9 (December 1978)

[14] Shipsey,E.J., Redmon,L.T., Browne,J.C., and Olson,R.E., Phys. Rev. A18 (1978) 1961

[15] Freeman,R.L., and Jones,E.M., Atomic Collision Processes in

Plasma Physics Experiments, Culham Lab. report CLM-R 137 (1974)

[16] Cordey,J.G., and Core,W.G.F., Phys. Fluids 17 (1974) 1626

[17] Lehner,G., Z. Physik 232 (1970) 172

[18] Towner,H.H., I.E.E.E. 1977 Intl. Conf. on Plasma Science, I.E.E.E. Conf. Records - Abstracts (1977) 92.

[19] Bayfield,J.E., and Khayrallah, G.A., Phys. Rev. A11 (1975) 920

[20] Jacobs, A., J. Quant. Spec. Radiat. Transfer 12 (1972) 243

[21] Allen,C.W., 'Astrophysical Quantities', Athlone Press, London, (1955) 64-68

[22] Medley,S. private communication

[23] Barnett,C.F., Ray,J.A., Ricci,E., Wilker,M.I., McDaniel,E.W., Thomas,E.W., and Gilbody,H.B., Atomic Data for Controlled Fusion Research, Oak Ridge Natl. Lab. report ORNL-5206 (February 1977)

[24] Marion,J.B., and Young,F.C., Nuclear Reaction Analysis, American Elsevier Publishing, New York (1968)

[25] Fedorenko,N.V., Soviet Phys. - Tech. Phys. 15 (1971) 1947.

[26] Riviere,A.C., and Sweetman,D.R., Bull. Am. Phys. Soc. 15 (1970) 1440

[27] Dimov,G.I., and Roslykov,G.V., Nucl. Fusion 15 (1975) 551

[28] Berkner,K.H., Morgan,T.J., Pyle,R.V., and Stearns,J.W. Phys. Rev. A8 (1973) 2870.

[29] Stearns,J.W., Berkner,K.H., and Pyle,R.V., Neutral Beam Design Options, Lawrence Berkeley Lab. report LBL-4492 (1976)

[30] Stearns,J.W., Berkner,K.H., Pyle,R.V., Briegleb,B.P., and Warren,M.L., Phys. Rev. A4 (1971) 1960.

[31] Ryding,G., Wittkower,A.B., and Rose,P.H., Phys. Rev. 174 (1968) 149.

[32] Allison,S.K., Cuevas,J., and Garcia-Munoz,M., Phys. Rev. 120 (1960) 1266.

[33] Prelec,K., Proc. of the Symp. on Production and Neutralization of Negative Hydrogen Ions and Beams, Brookhaven Natl. Lab. report BNL 50729 (1978)

TABLE I.

Beam Energies and Resonant Final States

Beam Species	Beam Energy (MeV)	Resonant $^4He^+$ state	Resonant $^4He^o$ state
H	0.2 - 0.9	2ℓ	
H_2	0.6 - 1.8	-	-
^3He	0.5 - 2.6	-	$1s^2$
^6Li	1.7 - 5.2	3ℓ	-

TABLE II.

TFTR Parameters

$n_e = 2n_D = 2n_T$	1×10^{14} cm^{-3}
T_e	10 keV
T_i	20 keV
v_c	4.5×10^8 cm sec^{-1}
$n_D n_T \langle \sigma v \rangle_{th}$	1×10^{12} cm^{-3} sec^{-1}
τ_s	400 msec
n_α	1×10^{12} cm^{-3}
ΔE_o	600 keV

TABLE III.

Radiative Decay and Ionization Rates

Excited State	Decay Transition	Decay Rate($10^8 sec^{-1}$)	Ionization Rate($10^8 sec^{-1}$)
$^4He^+$:			
2p	2p->1s	100	0.07
3d	3d->2p	10	0.5
4f	4f->3d	2.2	1.9
3p	3p->1s	26	0.5
4d	4d->3p	1	1.9
$^4He^o$ (singlet states) :			
1s2p	1s2p->$1s^2$	23	0.3
1s3p	1s3p->$1s^2$	5.6	2.1

TABLE IV.

Volume Source Rates and Fluences at a Detector for Reactions I-VI

Reaction	Beam	Beam Energy (MeV)	Beam Density (cm^{-3})	Volume Source Rate Photons cm^{-3} sec^{-1}	Fluence (10 degrees # cm^{-2} sec^{-1}
I	H°	0.88	10^8	$7.x10^{10}$	$6.3x10^7$
II	$H_2{}^{\circ}$	1.8	10^5	$1.4x10^8$	$1.26x10^5$
III	$^3He^{\circ}$	2.6	10^5	$1.9x10^8$	$1.71x10^5$
IV	Li°	6.1	10^5	$1.3x10^8$	$1.17x10^5$
				$^4He^{\circ}$ cm^{-3} sec^{-1} steradians $^{-1}$ at 10 degrees	
V	$H_2{}^{\circ}$	1.8	10^5	$2.7x10^7$	$3.05x10^5$
VI	$^3He^{\circ}$	2.6	10^5	$3.5x10^7$	$3.95x10^5$
VII	Li°	6.1		no cross section available	

Table V.

Neutral	Primary Ion	Neutralization Efficiency	Beam Density From Ion Source Considerations	Accelerator Current	Accelerator Power
0.9 MeV H°	0.9 MeV H^+	4×10^{-4} (a)	$2 \times 10^5/cm^3$		
0.9 MeV H°	0.9 MeV H^-	0.7 (b)	$1 \times 10^8/cm^3$ (c)	1 A (c)	1 MW (c)
1.8 MeV H_2°	1.8 MeV H_2^+	1×10^{-4} (a, d)	$2 \times 10^4/cm^3$	4 A	7 MW
1.8 Mev H_2°	2.6 MeV H_3^+	2×10^{-4} (a, d)	$4 \times 10^4/cm^3$	4 A	10 MW
2.6 MeV $^3He^\circ$	2.6 MeV $^3He^+$	1.5×10^{-3} (a)	$4 \times 10^5/cm^3$	1.5 A (e)	3.5 MW (e)
2.6 MeV $^3He^\circ$	3.5 MeV $^3HeH^+$	1.5×10^{-2} (a, d)	$2 \times 10^6/cm^3$	150 mA (e)	0.5 MW (e)
2.6 MeV $^3He^\circ$	2.6 MeV $^3He^-$	0.4 (f)	$3 \times 10^5/cm^3$	5 mA (e)	15 kW (e)
6 MeV Li°	6 MeV Li^+	1×10^{-4} (c)	$1 \times 10^4/cm^3$		
6 MeV Li°	6 MeV Li^-	0.5 (f)	$8 \times 10^6/cm^3$ (c)	4 mA (e)	25 kW (e)

NOTES:

a. Calculated from extrapolated cross sections

b. Measured

c. Assuming an average beam power density limit of 10 kW/cm^2

d. Using optimum neutralizer thickness

e. To supply the minimal $10^5/cm^3$ over 50 cm^2

f. Estimated

FIGURE CAPTIONS

Figure 1) a) Cross sections for the single charge transfer reactions I through IV (see text) as a function of the relative velocity and the corresponding energy $E_{He}=m_{\alpha}v^2_{rel}/2$. b) Cross sections for the double charge transfer reactions V and VI.

Figure 2) A schematic of velocity-space: the large circle represents the edge of the alpha-particle distribution, and the small circle indicates the relative size of v_{cutoff}.

Figure 3) The classical and non-classical alpha-particle distributions are shown as a function of alpha-particle speed (the vertical scale is arbitrary).

Figure 4) The values of $\langle\sigma v\rangle$ which follow from the a) classical and b) non-classical alpha distributions are shown as a function of v_{beam}.

Figure 5) The differential $\langle\sigma v\rangle$ for the a) classical and b) non-classical alpha distributions are shown as a function of the angle between the neutral particle detector and the neutral doping beam axis for several beam speeds. Results for reaction V are plotted with broken lines, solid lines are used for reaction VI.

Figure 6) The spectral intensities of the decay radiation from $(^4He^+)^*$ which follow from the a) classical and b) non-classical alpha distributions are shown as a function of the Doppler shift away from the nominal wavelength (for reactions I-III λ_o=304 Angstroms and for reaction IV λ_o=256 Angstroms) for four doping beam speeds: v_{beam}/v_o=1.0, 0.8, 0.6, 0.4. Arrows are plotted at the Doppler shift positions corresponding to the four speeds; the upper sets of arrows are appropriate for reactions I-III and the bottom sets apply to reaction IV.

Figure 7) The speed distributions of the escaping $^4He^o$ which follow from the a) classical and b) non-classical alpha distributions are shown for four beam speeds: v_{beam}/v_o=1.0, 0.8, 0.6, 0.4.

Figure 8) Schematic diagram of the beam-plasma-detector geometry as seen from above.

Figure 9) Schematic diagram of the reaction volume.

Figure 10) Interaction volume, V, and volume-source-rate to fluence conversion factors δ as a function of the angle, ϑ, between the beam and detector axes.

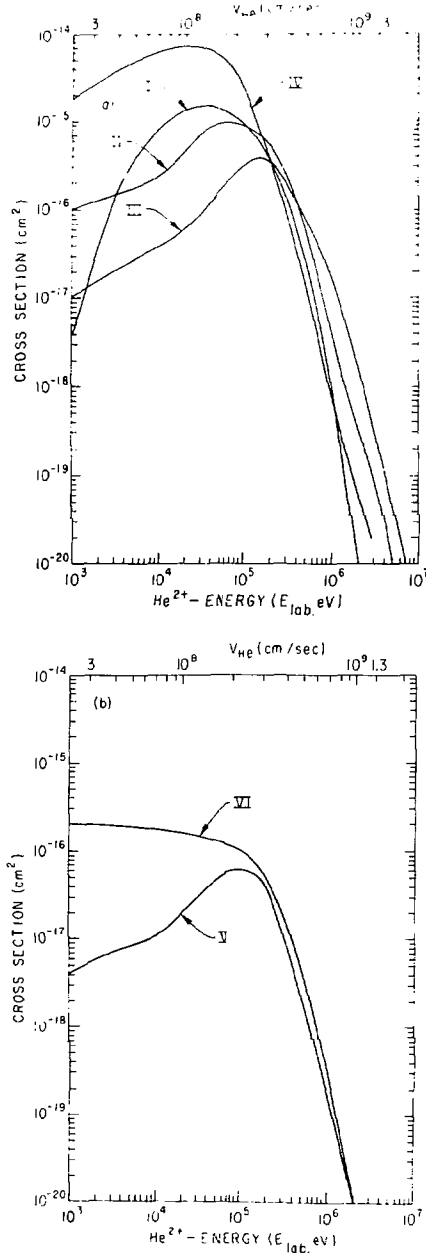

Fig. 1 792382

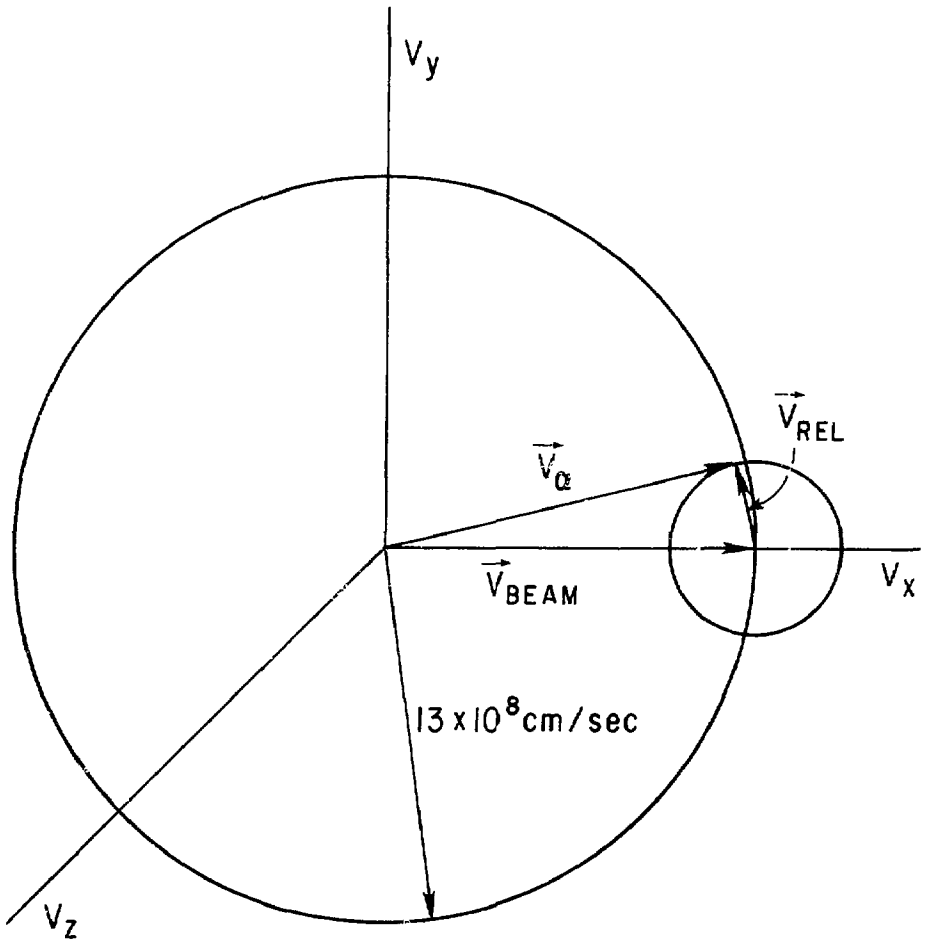

Fig. 2 792262

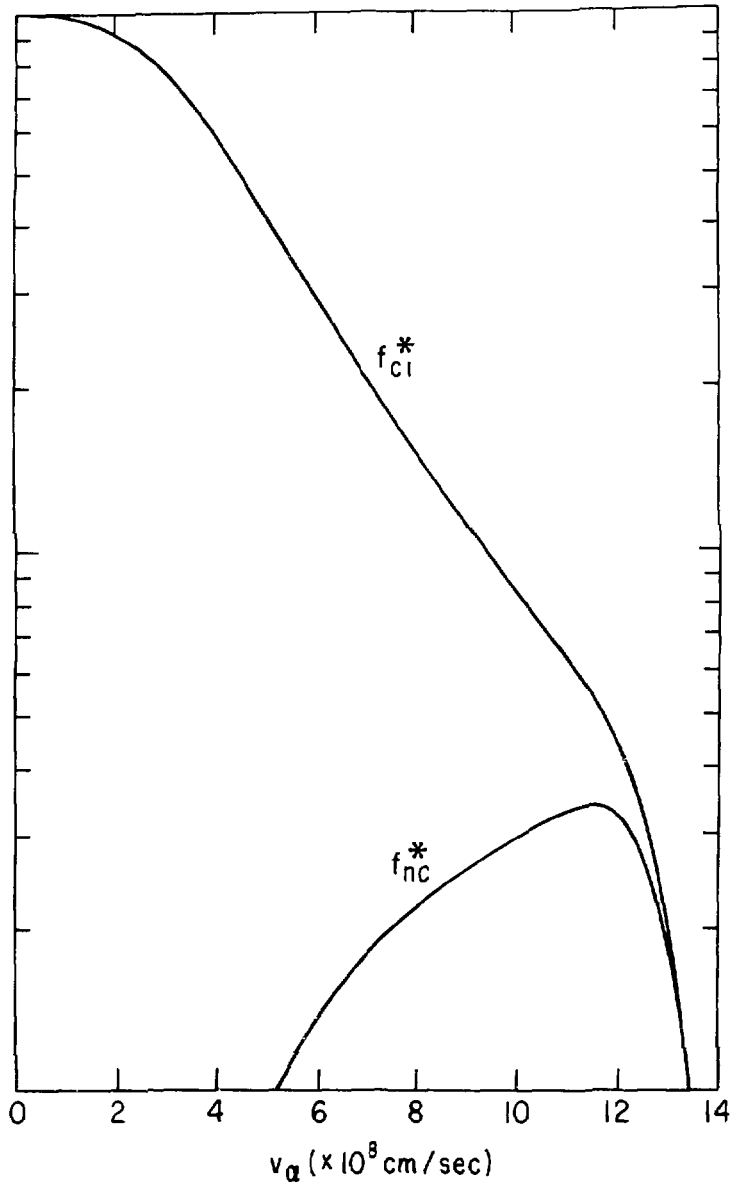

Fig. 3 792377

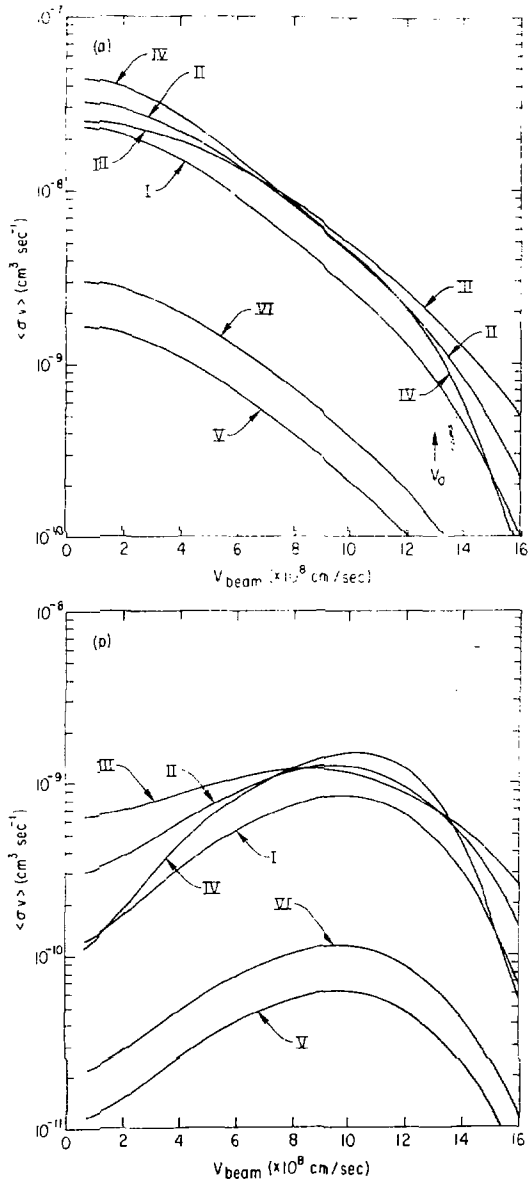
(a)
IV
II
III
I
VI
V
V_0
$\langle\sigma v\rangle$ (cm^3 sec^{-1})
V_{beam} (x10^8 cm/sec)
(p)
III
II
I
IV
VI
V
$\langle\sigma v\rangle$ (cm^3 sec^{-1})
V_{beam} (x10^8 cm/sec)

Fig. 4 792384

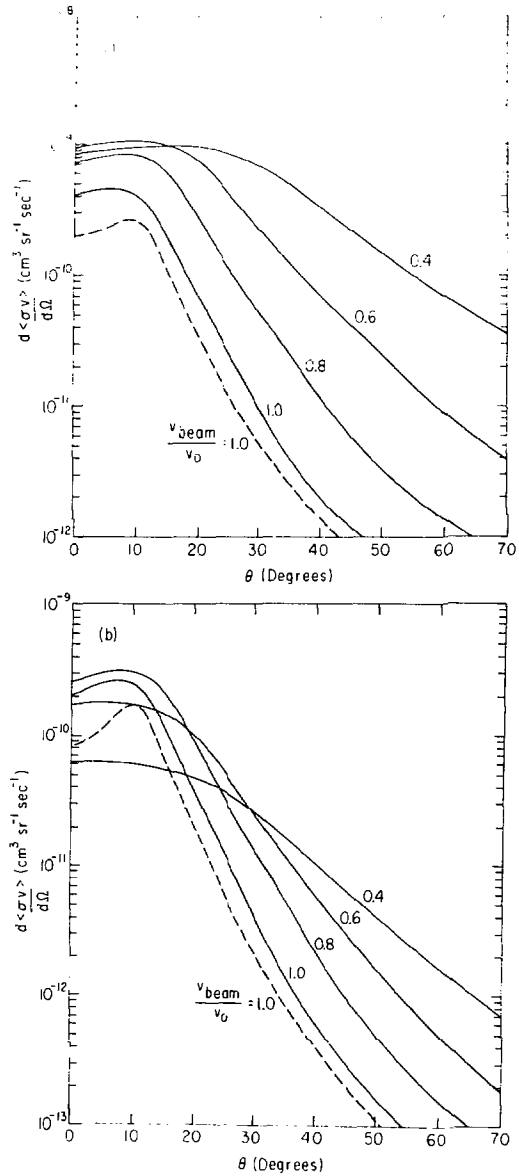
(b)
$d\langle\sigma v\rangle/d\Omega$ (cm^3 sr^{-1} sec^{-1})
θ (Degrees)
0.4
0.6
0.8
1.0
$\frac{v_{beam}}{v_0}$ = 1.0

Fig. 5 792379

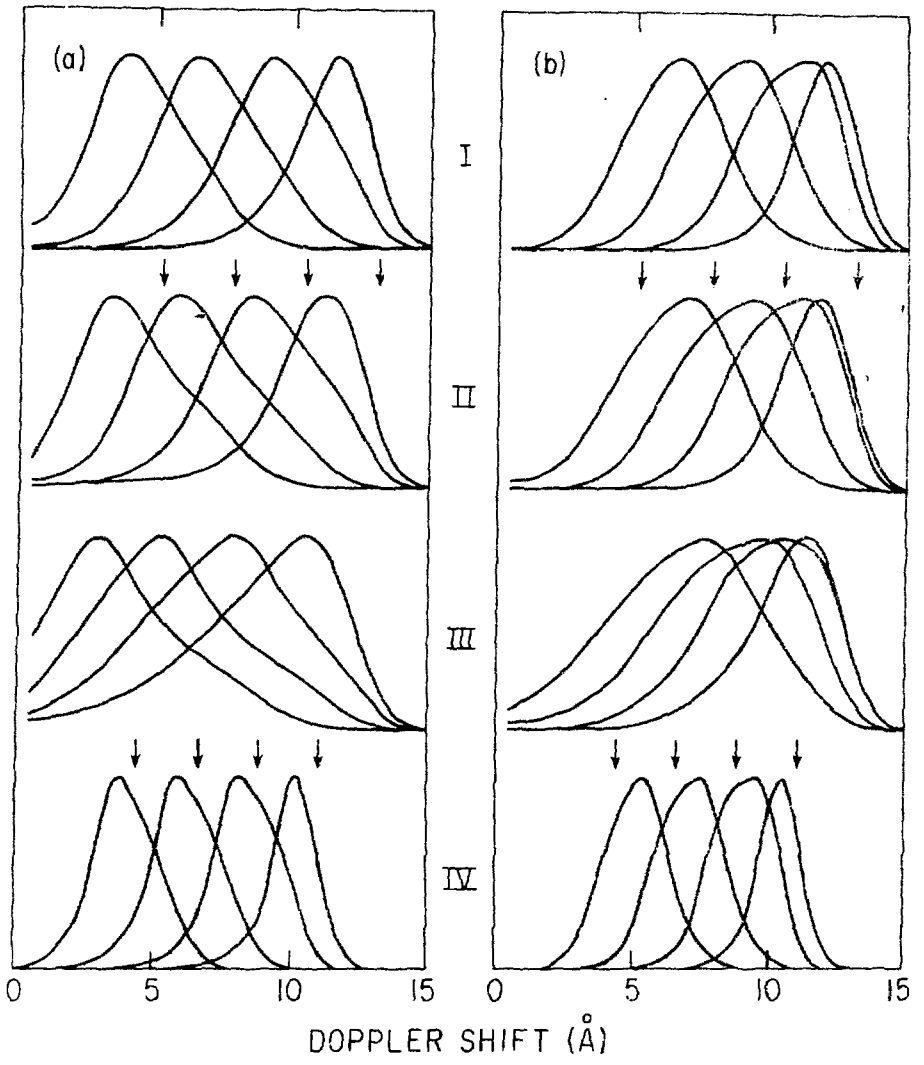

Fig. 6

792383

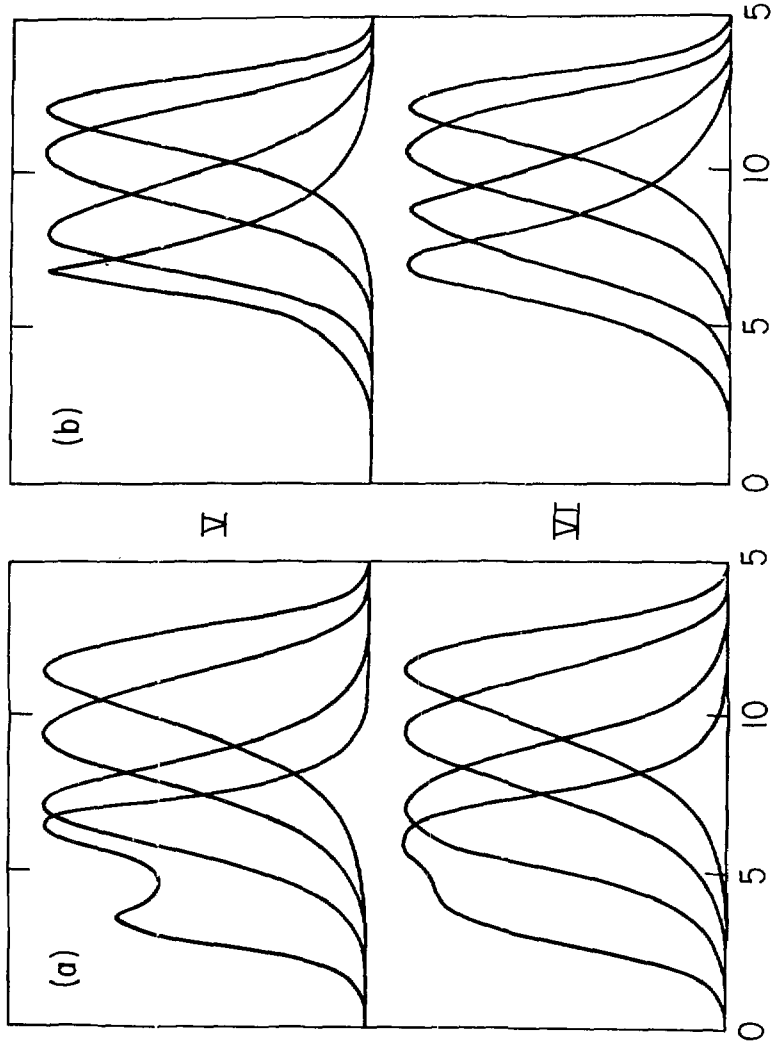

Fig. 7

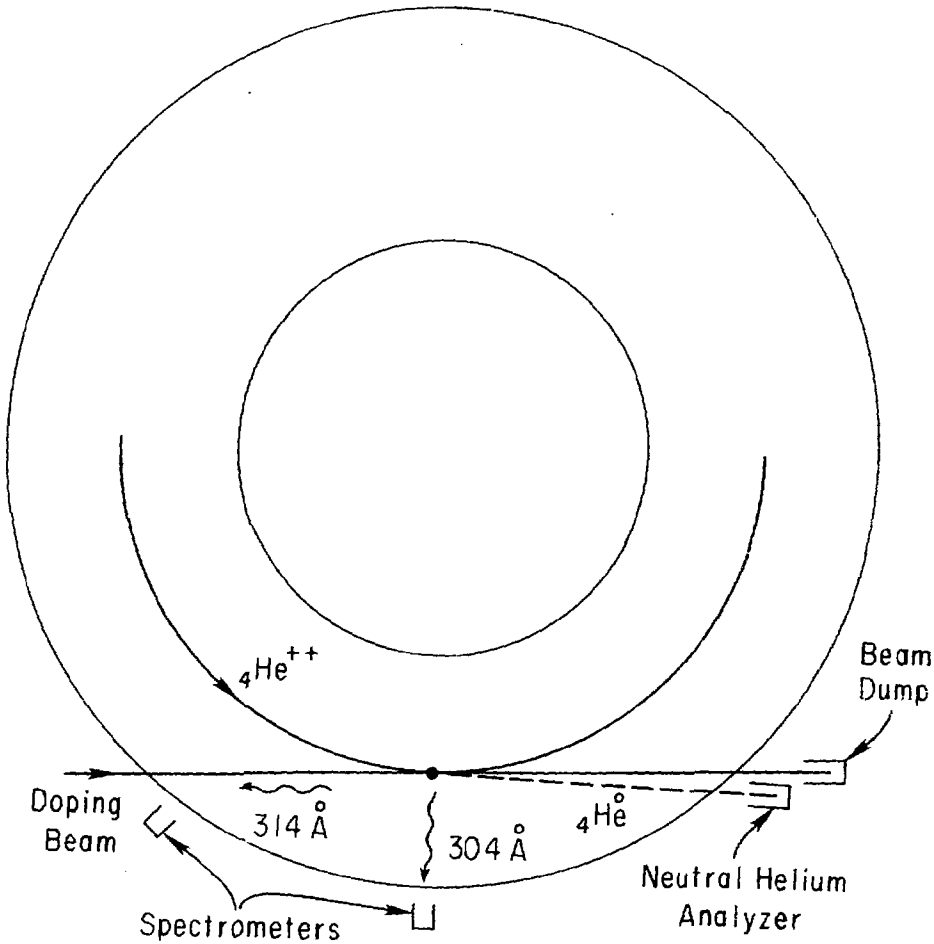
$_4He^{++}$
Beam Dump
Doping Beam
314 Å
304 Å
$_4\mathring{H}e$
Neutral Helium Analyzer
Spectrometers

Fig. 8

792380

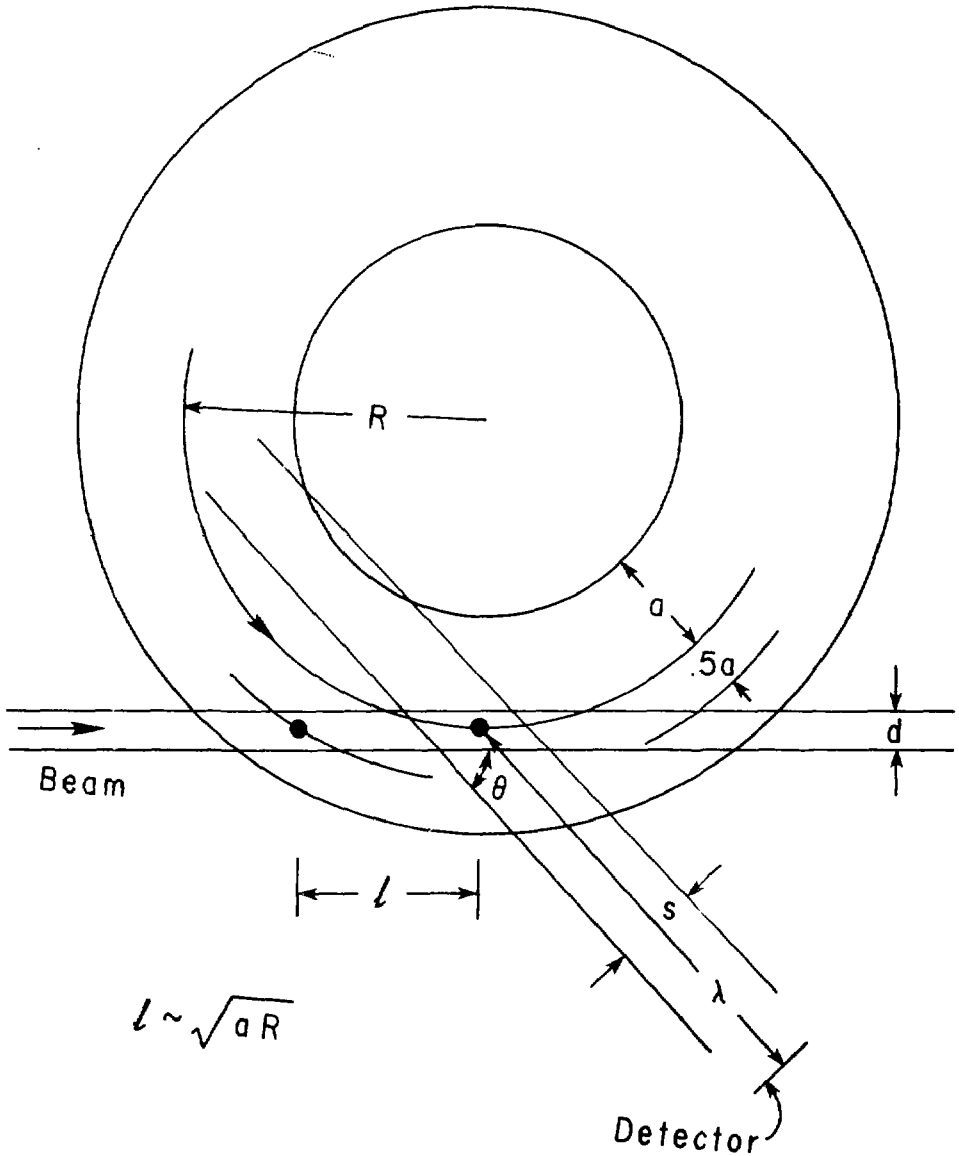

Fig. 9

792303

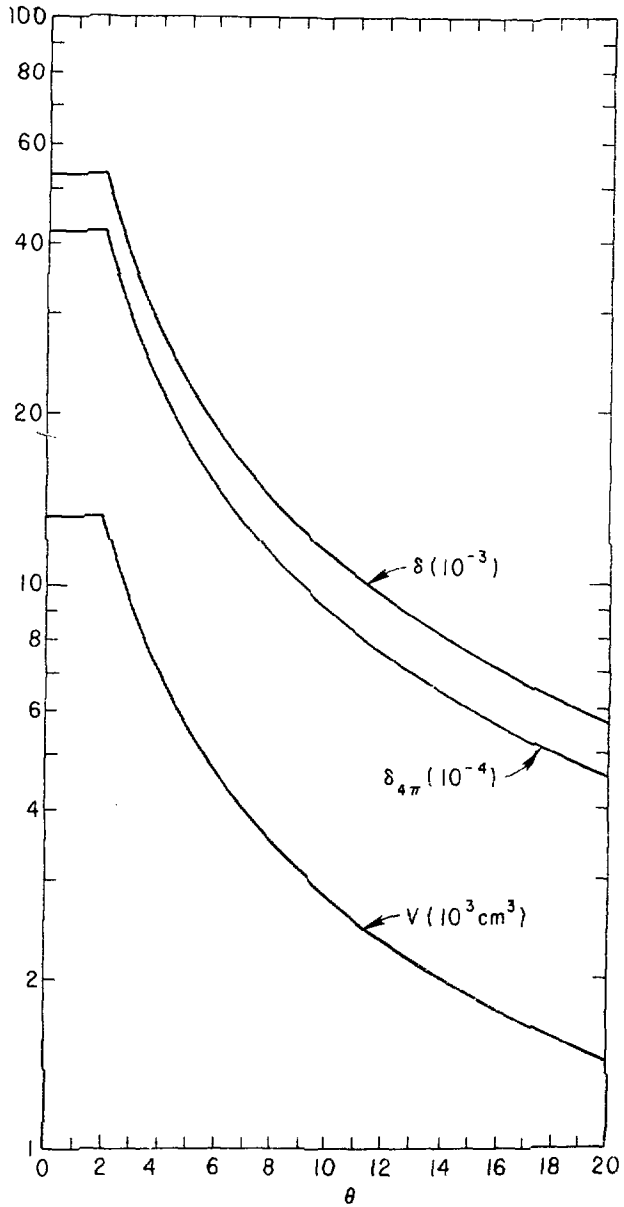

Fig. 10 792304